

An ab-initio many-body method for electronic structure calculations of solids. II. Unscreened Hartree-Fock treatment for the 3d systems Fe, Co, Ni and Cu

I. Schnell,^{1,2} G. Czycholl,² and R.C. Albers¹

¹*Theoretical Division, Los Alamos National Laboratory, Los Alamos, New Mexico 87545*

²*Department of Physics, University of Bremen, P.O.Box 330 440, D-28334 Bremen, Germany*

(Dated: September 28, 2018)

The ab-initio many-body method suggested in the preceding paper is applied to the 3d transition metals Fe, Co, Ni, and Cu. We use a linearized muffin-tin orbital calculation to determine Bloch functions for the Hartree one-particle Hamiltonian, and from these obtain maximally localized Wannier functions. Within this Wannier basis all relevant one-particle and two-particle Coulomb matrix elements are calculated. The resulting second-quantized many-body Hamiltonian with ab-initio parameters is studied within the simplest many-body approximation, namely the unscreened, selfconsistent, Hartree-Fock approximation (HFA). We present these HFA results, which we believe are the first to have been done for crystalline 3d transition metals, and compare them with those obtained from the standard local (spin) density approximation (LSDA) within density functional theory (DFT). Although the d-bands sit considerably lower within HFA than within LSDA, the exchange splitting and magnetic moments for ferromagnetic Fe, Co, and Ni are only slightly larger in HFA than what is obtained experimentally or within LSDA. The HFA total energies are lower than the corresponding LSDA calculations.

PACS numbers: 71.10.Fd, 71.15.AP, 71.15.Mb, 71.20.Be, 71.45.Gm, 75.10.Lp

I. INTRODUCTION

In the preceding paper¹ we suggested a new method for ab-initio electronic-structure calculations of solids. The main steps of this procedure are:

1. Perform a conventional, self-consistent, band-structure calculation for an effective one-particle Hamiltonian, namely, the Hartree Hamiltonian, to obtain a suitable basis set of Bloch functions.
2. By taking into account only a finite number J of bands one chooses a truncated one-particle Hilbert space. The Marzari-Vanderbilt² algorithm is then used to construct a maximally localized set of Wannier functions, which span the same truncated one-particle Hilbert space.
3. All one-particle (tight-binding) and two-particle (Coulomb) matrix elements of the Hamiltonian within this Wannier function basis are calculated.
4. The resulting electronic many-body Hamiltonian in second quantization with parameters determined from first principles is studied within standard many-body approximations for lattice electron systems.

In this paper we apply this scheme to the 3d transition metals Fe, Co, Ni, and Cu. We use the “linear muffin-tin orbital” (LMTO) method within the “atomic-sphere approximation” (ASA)³ to perform the band-structure calculation for the Hartree Hamiltonian in first quantization. The direct Coulomb matrix elements of the maximally localized Wannier basis are rather large, about 20 eV in magnitude. We then use the simplest possible

many body approximation, the Hartree-Fock approximation (HFA), to study the second-quantized multiple-band Hamiltonian. Our results are compared with those obtained from a standard LSDA calculation.^{4,5} Although the 3d-bands and the 4s-band overlap in the LSDA approximation, our unscreened HFA calculations give 3d-bands that lie considerably lower (between 10 and 20 eV) than the 4s-band. The HFA correctly predicts ferromagnetism for the ferromagnetic metals Fe, Co, and Ni and no magnetism for Cu, but with a much larger exchange splitting between majority and minority 3d bands than obtained within LSDA and with a slightly larger magnetic moment per site than obtained experimentally or within LSDA. On the other hand, the total energy is lower in HFA than in LSDA. The LSDA results for metals are probably more reliable than our new HFA results, which lack important screening and correlation effects. In order for our method to go beyond LSDA we would need to use better many body methods than the (unscreened) HFA, which should be possible within our scheme.

Our purpose in presenting the HFA results is to demonstrate that the new ab-initio many-body method that we have proposed is feasible and can be applied to practical calculations of materials. In addition, because HFA is the assumed standard starting point before adding complex many-body correlations, and because it is the simplest many-body approximation (or the best mean-field one-particle approximation), it is useful to know what the HFA predicts for the 3d transition metals, which have been so heavily studied by other techniques. Comparisons of HFA results with experiments, other (higher order) theories, or established standard methods such as the LSDA should demonstrate the effects of correlation on electronic properties in d-electron systems.

To the best of our knowledge we do not know of any published HFA results (band structure, density of states, magnetism, magnetic moment, total energy, etc.) for the 3d ferromagnets Fe, Co and Ni, unless it was implicitly applied to these materials for schemes like the local ansatz⁶, where HFA results serve as an input to higher order calculations. This is not surprising since the HFA has, from very early on, been viewed as a poor approximation for metals. For example, when applied to the homogeneous electron gas (as the simplest model of an infinite metallic system), the HFA has well-known Fermi edge singularities^{7,8}. These lead, in particular, to a vanishing density of states (DOS) at the Fermi energy, which is, of course, unphysical. This unphysical feature usually prevails in actual HFA-calculations for real metals⁹, though sometimes this singularity is hard to see in actual HFA-results¹⁰. In our calculations the non-locality is handled through the calculation of expectation values (matrix elements of the density matrix), which makes HF calculations as easy as Hartree calculations. Furthermore, because of our localized Wannier basis, we only keep on-site and a few inter-site Coulomb and exchange matrix elements. Hence our calculations have an effective short-ranged Coulomb interaction. Although longer-range Coulomb matrix elements are small in our calculations, which is why we truncate them, it is possible that if all of them were kept to infinite distances that they could add up to give Fermi edge singularities (which are due to the long-ranged nature of the bare Coulomb interaction) and other standard anomalies. Correlation or screening would quickly kill these effects.

The paper is organized as follows. In Section II we describe the LMTO-Hartree calculations and the Hartree-results for the band structure and density of states, respectively. Section III describes some results obtained for the maximally localized Wannier functions obtained within the Marzari-Vanderbilt algorithm², in particular their localization properties. Results for the matrix elements, in particular the direct Coulomb and exchange matrix elements are given in Section IV; we also compare these results with calculations of the Slater integrals. The application of the (unscreened) HFA to the multiband many-body Hamiltonian in second quantization is the subject of Section V. For an interpretation of the results we compare the numerical HFA results obtained for the crystal with previous atomic HFA results and with numerical and analytical results for a simplified local (atomic or zero band width) model in Section VI. A comparison with the more standard LSDA-results follows in Section VII, before the paper closes with a short discussion.

II. LMTO HARTREE CALCULATION

For the four materials of interest (Fe, Co, Ni, Cu) we performed a selfconsistent Hartree band-structure calculation. Besides the nuclear charge we used the (experi-

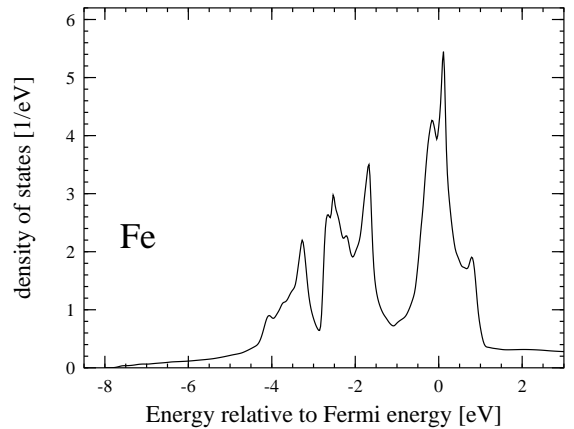


FIG. 1: Total density of states (of both spin directions) around the Fermi level (chosen as zero of the energy axis $E_F = 0$) obtained from the selfconsistent Hartree calculation for Fe.

mentally) known results for the lattice structure (bcc for Fe, fcc otherwise; Co should actually be hexagonal) and for the lattice constant as input. For the band-structure calculation we used the LMTO method^{3,11} within the atomic sphere approximation (ASA). The radius of the (overlapping) muffin-tin spheres (the Wigner-Seitz radius S) is determined by the condition that the sphere volume equals the volume of the unit cell. This yields the following values for the Wigner-Seitz radius: $S = 2.662a_0$ for Fe, $S = 2.621a_0$ for Co, $S = 2.602a_0$ for Ni and $S = 2.669a_0$ for Cu (Ref. 3). Within the muffin-tin spheres the potential and wave functions are expanded in spherical harmonics with a cutoff $l_{\max} = 2$, i.e., s, p, and d-orbitals are included.

Within the LMTO-ASA the eigenfunctions, i.e. the Bloch wave functions (inside a muffin-tin sphere), are given in terms of the solution to the radial Schrödinger equation $\phi_{\nu l}(r)$ to some fixed energies $E_{\nu l}$ and its energy derivative $\dot{\phi}_{\nu l}(r)$:

$$\Psi_{n\mathbf{k}}(\mathbf{r}) = \sum_L \left(\phi_{\nu l}(r) A_L^{n\mathbf{k}} + \dot{\phi}_{\nu l}(r) B_L^{n\mathbf{k}} \right) Y_L(\hat{\mathbf{r}}) , \quad (1)$$

where the $Y_L \equiv Y_l^m$ denote the (complex) spherical harmonics and n is the band index.

Figs. 1 - 4 show the nonmagnetic (spin-degenerate) Hartree results for the density of states (DOS). One observes that the five narrow 3d-bands are similar in energy and therefore hybridize with the 4sp-bands. For Fe, Co, and Ni the Fermi level E_F falls in the midst of the partially filled 3d-bands, and hence there is a large DOS at the Fermi level. For Cu E_F is above the filled 3d bands, where the states have more 4sp-like character and the DOS is small (free electron like).

The Bloch functions obtained from this Hartree calculation are used as the basis of a truncated Hilbert space. In the band calculation, there is already a natural truncation due to the spherical harmonics expansion cutoff

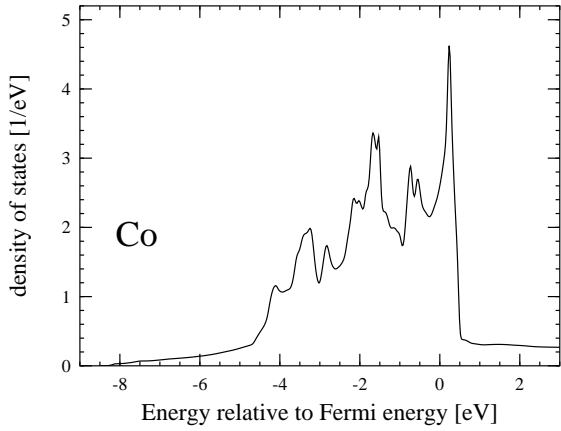


FIG. 2: The same as in Fig. 1 for Co.

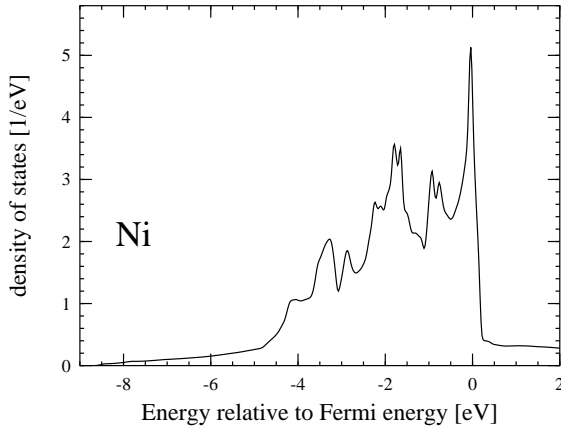


FIG. 3: The same as in Fig. 1 for Ni.

$l_{max} = 2$, which limits the calculation to 9 bands for one atom per unit cell. The connection between the Bloch functions in the different muffin-tin spheres is given by the standard Bloch relation

$$\psi_{n\mathbf{k}}(\mathbf{r} + \mathbf{R}) = e^{i\mathbf{k}\mathbf{R}} \psi_{n\mathbf{k}}(\mathbf{r}) . \quad (2)$$

Hence the Bloch function in a single muffin-tin sphere determines the function for the whole crystal. However, this simple relation holds for Bloch functions only. Any other function (to be represented as linear combination of Bloch functions) can, nevertheless, be decomposed into its contributions within the different muffin-tins according to

$$\Phi_\alpha(\mathbf{r}) = \sum_i \Phi_\alpha(\mathbf{R}_i; \mathbf{r} - \mathbf{R}_i) \quad (3)$$

where $\Phi_\alpha(\mathbf{R}; \mathbf{r}) = 0$ for $|\mathbf{r}| > S$.

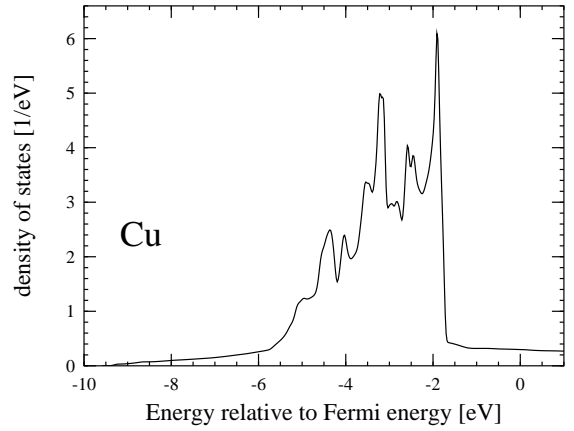


FIG. 4: The same as in Fig. 1 for Cu.

III. MAXIMALLY LOCALIZED WANNIER FUNCTIONS

We now turn to the construction and description of the Wannier functions and will present results for their main properties for the four materials under investigation. Because

$$w_{\mathbf{R}n}(\mathbf{r}) = w_{\mathbf{0}n}(\mathbf{r} - \mathbf{R}) , \quad (4)$$

it is sufficient to investigate the Wannier functions only for one arbitrarily chosen lattice vector $\mathbf{0}$: $w_n(\mathbf{r}) \equiv w_{\mathbf{0}n}(\mathbf{r})$. This Wannier function has contributions not only in the muffin-tin sphere around $\mathbf{0}$ but also in other muffin-tin spheres, and we can use the decomposition (3) into the contributions from the different muffin-tin spheres

$$w_n(\mathbf{r}) = \sum \mathbf{w}_n(\mathbf{R}; \mathbf{r} - \mathbf{R}) . \quad (5)$$

After application of the Marzari-Vanderbilt algorithm, which is briefly summarized in the preceding paper¹ and in more detail in Ref. 2, the new set of bands that are used to calculate the maximally localized Wannier functions can no longer be classified by pure angular momentum quantum numbers. The Wannier functions are rather admixtures having different L -contributions (3d, 4s, 4p etc.). But, since the original Bloch functions from which the Wannier functions are constructed were given in terms of a spherical harmonics expansion, the new Wannier functions (and their contribution in each individual muffin-tin sphere) can also be decomposed into these spherical harmonics contributions

$$w_n(\mathbf{R}; \mathbf{r}) = \sum_L \left\{ \phi_{\nu l}(r) A_L^{\mathbf{R}n} + \dot{\phi}_{\nu l}(r) B_L^{\mathbf{R}n} \right\} Y_L(\hat{\mathbf{r}}) . \quad (6)$$

One can then calculate the weight of the contributions to the Wannier function (centered at $\mathbf{0}$) within the different muffin-tin spheres

$$\langle w_n | w_n \rangle_{\mathbf{R}} \equiv \int_{\mathbf{R}} d^3 \mathbf{r} |w_n(\mathbf{r})|^2 = \int_0 d^3 \mathbf{r} |w_n(\mathbf{R}; \mathbf{r})|^2 , \quad (7)$$

n	0	1	2	3	4	5	6	7
$\sum_l C_l^{0n}$.9761	.9765	.9596	.9800	.9773	.8754	.8731	.8763
$\sum_{\mathbf{R}} C_{l=0}^{\mathbf{R}n}$.0019	.0018	.0081	.0019	.0017	.2224	.2381	.2265
$\sum_{\mathbf{R}} C_{l=1}^{\mathbf{R}n}$.0955	.0726	.1797	.0611	.0728	.5480	.5509	.5347
$\sum_{\mathbf{R}} C_{l=2}^{\mathbf{R}n}$.9026	.9256	.8121	.9370	.9255	.2295	.2110	.2388

TABLE I: Some properties of the lowest eight maximally localized Wannier functions of Fe.

and one can also decompose this into the different l -contributions according to:

$$\langle w_n | w_n \rangle_{\mathbf{R}} = \sum_l \underbrace{\sum_{m=-l}^l \left\{ |A_{lm}^{\mathbf{R}n}|^2 + \langle \phi_{nl}^2 \rangle |B_{lm}^{\mathbf{R}n}|^2 \right\}}_{\equiv C_l^{\mathbf{R}n}} \quad (8)$$

For the 3d-system iron these quantities are tabulated in Table I. The first line is the weight $\langle w_n | w_n \rangle_{\mathbf{0}}$ in the center muffin-tin. Between 88 and 98% of the total weight of the Wannier functions is to be found already within the center muffin-tin; this shows how well localized our Wannier functions are with the lowest five functions having values of more than 95%. Rows 2–4 in this table indicate the different l -contribution or l -character of the Wannier functions. One sees that the optimally localized Wannier functions are not pure within their l -character, but the lowest five Wannier functions (0–4) still have mainly $l = 2$ (3d) character. Higher band-index states (which are slightly less well localized according to row 1) are admixtures that have mainly $l = 1$ (4p) character (about 50 %), but also a considerable amount of $l = 0$ (4s) and $l = 2$ (3d) character. Corresponding results for the other 3d-systems Co, Ni, and Cu are similar and, therefore, not repeated here.

IV. ONE PARTICLE AND COULOMB MATRIX ELEMENTS

From the optimally localized Wannier functions we calculate the one-particle matrix elements

$$t_{12} = \int d^3 \mathbf{r} w_1^*(\mathbf{r}) \left(-\frac{\hbar^2}{2m} \nabla^2 + V(\mathbf{r}) \right) w_2(\mathbf{r}) \quad (9)$$

and the Coulomb matrix elements of the Hamiltonian

$$W_{12,34} = \int d^3 \mathbf{r} d^3 \mathbf{r}' w_1^*(\mathbf{r}) w_2^*(\mathbf{r}') \frac{e^2}{|\mathbf{r} - \mathbf{r}'|} w_3(\mathbf{r}') w_4(\mathbf{r}) \quad (10)$$

Here we use the abbreviated notation 1 to mean $\mathbf{R}_1 n_1$ and 2 to mean for $\mathbf{R}_2 n_2$, etc. We used two different numerical algorithms to calculate these Coulomb matrix elements, namely the FFT-algorithm briefly described in the previous paper and a spherical expansion algorithm described in some detail in Ref. 12. The latter method makes use of the fact that (in each muffin-tin sphere) the

U_{nm}	0	1	2	3	4	5	6	7	8
0	22.42	20.90	20.10	20.96	20.86	14.16	13.32	13.96	13.50
1	20.90	23.04	19.95	21.55	21.53	14.07	13.54	13.58	14.15
2	20.10	19.95	20.77	20.05	19.83	12.95	13.46	13.37	13.22
3	20.96	21.55	20.05	23.27	21.67	13.46	14.05	13.98	13.98
4	20.86	21.53	19.83	21.67	22.99	13.71	13.28	14.25	14.12
5	14.16	14.07	12.95	13.46	13.71	13.67	9.45	9.58	9.64
6	13.32	13.54	13.46	14.05	13.28	9.45	13.52	9.27	9.50
7	13.96	13.58	13.37	13.98	14.25	9.58	9.27	13.75	9.65
8	13.50	14.15	13.22	13.98	14.12	9.64	9.50	9.65	13.81

J_{nm}	0	1	2	3	4	5	6	7	8
0	22.42	0.84	0.61	0.75	0.99	0.86	0.73	0.81	0.42
1	0.84	23.04	0.77	0.88	0.84	0.70	0.51	0.48	0.86
2	0.61	0.77	20.77	0.88	0.70	0.96	0.93	0.92	0.60
3	0.75	0.88	0.88	23.27	0.82	0.33	0.78	0.64	0.69
4	0.99	0.84	0.70	0.82	22.99	0.52	0.46	0.75	0.83
5	0.86	0.70	0.96	0.33	0.52	13.67	0.58	0.56	0.57
6	0.73	0.51	0.93	0.78	0.46	0.58	13.52	0.45	0.56
7	0.81	0.48	0.92	0.64	0.75	0.56	0.45	13.75	0.55
8	0.42	0.86	0.60	0.69	0.83	0.57	0.56	0.55	13.81

TABLE II: On-site direct and exchange Coulomb matrix elements between Wannier functions for Fe. All energies are eV's.

Wannier functions are explicitly given as linear combinations of products of spherical harmonics and a radial wave function. The expansion

$$\frac{1}{|\mathbf{r} - \mathbf{r}'|} = \sum_{k=0}^{\infty} \frac{4\pi}{2k+1} \frac{r_<^k}{r_>^{k+1}} \sum_{m=-k}^k Y_K^*(\hat{\mathbf{r}}') Y_K(\hat{\mathbf{r}}) \quad (11)$$

($K = \{k, m\}$) makes it possible to express the on-site Coulomb integrals as one-dimensional integrals over products of the radial functions and the (tabulated) Gaunt coefficients. The results obtained by this algorithm and by the independent FFT-algorithm agree within the numerical errors (of at most 1%).

Results for the on-site direct and exchange Coulomb matrix elements between the optimally localized Wannier functions are given in Table II for iron (Fe). The direct Coulomb integrals $U_{nm} = W_{nm,mn}$ between the Wannier states with the lowest five band indices ($n, m \in \{0, \dots, 4\}$), which according to the discussion and table in the preceding section have mainly 3d-character, are rather large, up to 23 eV for Fe. Within the 3d-like bands the interband direct Coulomb matrix elements are of the same magnitude as the intraband matrix elements. The matrix elements between 3d-states and 4sp-states are considerably smaller, of the magnitude of 13 – 14 eV. For electrons in 4sp-states ($n, m \in \{5, \dots, 9\}$) the direct intraband Coulomb matrix elements are again of the order of 13 – 14 eV, but the interband matrix elements are

	U	J	t_{NN}	t_{NNN}
Fe	21.1	.81	.59	.24
Co	22.6	.87	.55	.10
Ni	22.6	.88	.75	.11
Cu	24.5	.94	.80	.12

TABLE III: Averaged on-site Coulomb, exchange, nearest neighbor and next nearest neighbor hopping matrix elements for the 4 3d-systems; energies are in eV.

	F^0	F^2	F^4
Fe (crystal)	21.62	9.61	5.91
Fe (atom [14])	23.76	10.96	6.81
Co (crystal)	23.18	10.31	6.34
Co (atom [14])	25.15	11.58	7.20
Ni (crystal)	24.69	11.00	6.77
Ni (atom [14])	26.53	12.20	7.58
Cu (crystal)	26.27	11.72	7.23
Cu (atom [14])	27.90	12.82	7.96

TABLE IV: Slater integrals F^k (in eV) for the 3d-systems Fe, Co, Ni, Cu as obtained by our calculations and within an earlier atomic calculation¹⁴.

slightly smaller, about 9 eV. The exchange matrix elements $J_{nm} = W_{nm,nm}$ are always much smaller, usually less than 1 eV (for $n \neq m$). Again the corresponding results for the other 3d-systems investigated (Co, Ni and Cu) are very similar.

For the 5 states with predominant 3d-character we have calculated the averages of the on-site direct and exchange Coulomb matrix elements

$$U \equiv \frac{1}{25} \sum_{mm'} W_{mm'm'm} \quad (12)$$

$$J \equiv \frac{1}{20} \sum_{m \neq m'} W_{mm'mm'} , \quad (13)$$

as well as the averages of the absolute values of the nearest neighbor (NN) and next nearest neighbor (NNN) hopping matrix elements

$$t_{NN(N)} \equiv \frac{1}{25} \sum_{n,m} |t_{Rnm}| . \quad (14)$$

The results obtained thereby for the 4 transition metals under consideration are shown in Table III. The U-values vary between 21 eV for Fe and 25 eV for Cu, the J-values are smaller than 1 eV and the hopping matrix elements are of the magnitude 0.5 – 0.7 eV for nearest-neighbor (NN) and 0.1 – 0.2 eV for next-nearest-neighbor (NNN), and further on decrease with increasing distance.

We have also evaluated the Slater integrals¹³:

$$F^k \equiv e^2 \int dr r^2 \int dr' r'^2 |R_{l=2}(r)|^2 \frac{r^k_{<}}{r^k_{>}} |R_{l=2}(r')|^2 , \quad (15)$$

where $R_{l=2}(r)$ is a radial (atomic) d-wave function (obtained by solving the Schrödinger equation for a radial symmetric potential, for instance). Note that only the three integrals F^0 , F^2 and F^4 are required to determine all the Coulomb d-matrix elements. Using the radial d-wave function obtained from the Hartree calculation we obtain the following values for the Slater integrals of the four 3d-systems: $F^0 = 21.62$ eV for Fe, 23.18 eV for Co, 24.69 eV for Ni, and 26.27 eV for Cu. This means, the Slater integrals F^0 are rather good estimates of our (averaged) Coulomb matrix elements. These values are also in agreement with older results obtained in calculations for 3d-atoms¹⁴. In Table IV we show our F^k -values for the four 3d-crystals and compare them with corresponding atomic calculations from Ref. 14. Obviously, there is fairly good agreement between these atomic and our results.

V. UNSCREENED HARTREE-FOCK APPROXIMATION

After we have determined the matrix elements within our restricted basis set of 9 maximally localized Wannier functions (per site and spin), we have a Hamiltonian in second quantization of the form

$$H = \sum_{12\sigma} t_{12} c_{1\sigma}^\dagger c_{2\sigma} + \frac{1}{2} \sum_{1234\sigma\sigma'} W_{12,34} c_{1\sigma}^\dagger c_{2\sigma'}^\dagger c_{3\sigma'} c_{4\sigma} \quad (16)$$

for which all the matrix elements are known from first principles. The simplest approximation one can now apply is the HFA, which replaces the many-body Hamiltonian by the effective one-particle Hamiltonian

$$H_{HF} = \sum_{12\sigma} (t_{12} + \Sigma_{12,\sigma}^{HF}) c_{1\sigma}^\dagger c_{2\sigma} \quad (17)$$

$$\text{with } \Sigma_{12,\sigma}^{HF} = \Sigma_{12}^{Hart} + \Sigma_{12,\sigma}^{Fock} \quad (18)$$

$$= \sum_{34\sigma'} [W_{13,42} - \delta_{\sigma\sigma'} W_{31,42}] \langle c_{3\sigma'}^\dagger c_{4\sigma'} \rangle .$$

Here the expectation values $\langle c_{1\sigma}^\dagger c_{2\sigma} \rangle$ have to be determined selfconsistently for the HF Hamiltonian (17). Note that the Fock (exchange) term is spin (σ) dependent and may, therefore, give rise to magnetic solutions.

The Hartree-Fock results for the four materials of interest are shown in Figs. 5–12. We show the effective HF band structure and its density of states (DOS). In our HFA calculations there are no singularities (or a vanishing DOS) at the Fermi level since we start from a localized description and consider the Coulomb matrix elements only locally (on-site and for a few neighbor shells). Therefore, we implicitly truncate the Coulomb interaction in real space and in practice work with an effective short-ranged interaction. Within HFA the main part of the 3d-bands lies between 18 and 22 eV below the Fermi level and is separated from the 4sp-bands. We find magnetism in HFA for Fe, Co, and Ni in agreement with

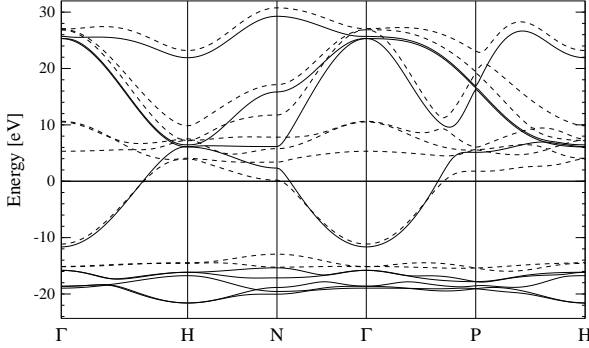


FIG. 5: (Unscreened) Hartree-Fock band-structure of Fe; the full line shows the majority (spin up), the dashed line the minority spin component.

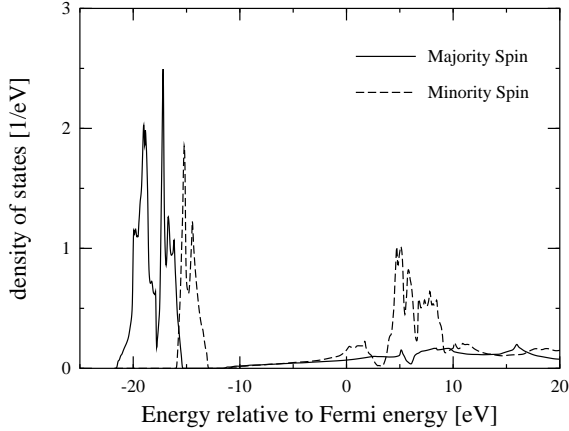


FIG. 6: Density of states (per spin direction) for Fe within the (unscreened) Hartree-Fock approximation; the full line shows the majority (spin up), the dashed line the minority spin contribution.

experiment. The five majority spin d-bands are about 20 eV below the Fermi energy and are completely filled. But the partially filled minority d-bands have two (for Fe), three (for Co), and four (for Ni) filled bands between -18 and -15 eV, and the rest are around and above the Fermi level. This results in magnetic moments per atom (in units of the Bohr magneton μ_B /atom) of 2.9 for iron, 1.9 for cobalt, and 0.76 for nickel. For copper no magnetism and exchange splitting of the 3d-bands is obtained, but the (spin degenerate) 3d-bands are at about 22 eV below the Fermi level and separated from the 4sp-bands. If we compare these results with the results of the simple Hartree approximation shown in Figs. 1–4 we see that the exchange term has two effects: it produces an exchange splitting and the possibility of magnetic solutions, and it draws the 3d-bands energetically down by an amount of about 20 eV. Compared with experiment the HFA overestimates magnetism and leads to overly large values for the magnetic moment per site (about 10–30% too large; experiment gives magnetic moments of about

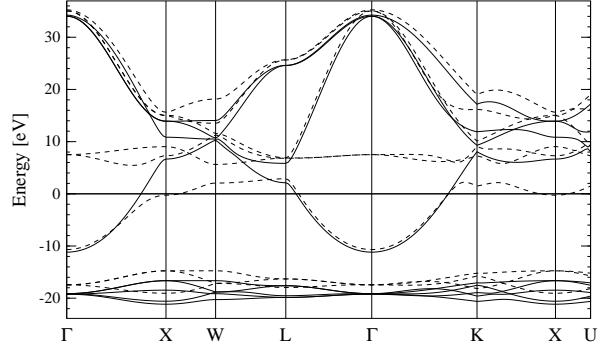


FIG. 7: The same as Fig. 5 for Co.

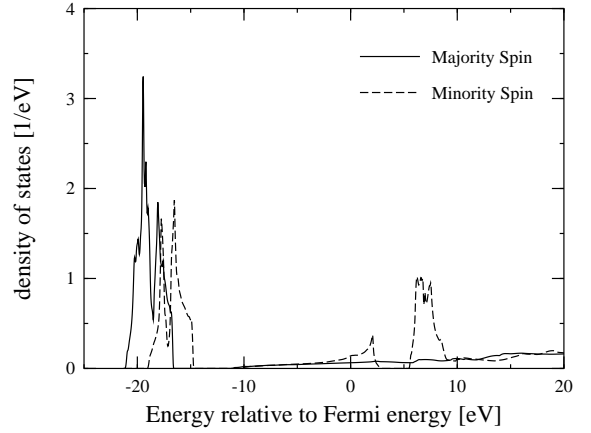


FIG. 8: The same as Fig. 6 for Co.

2.2 for iron, 1.7 for Co, and 0.6 for Ni). This is consistent with Heisenberg or Ising model studies where the mean-field approximation HFA also has the tendency to overestimate magnetism and magnetic solutions.

However, the reason why the 3d-bands lie so far below the Fermi level and the 4sp-band in HFA has nothing to do with the existence and overestimation of mag-

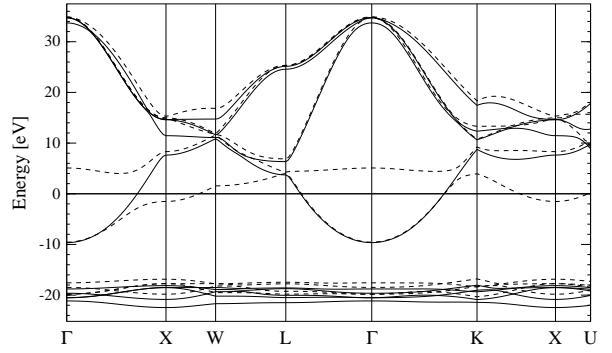


FIG. 9: The same as Fig. 5 for Ni.

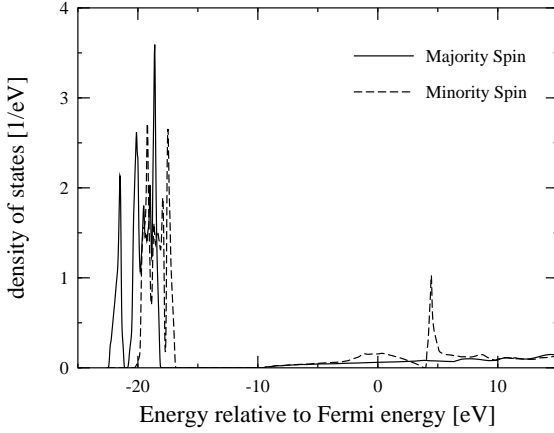


FIG. 10: The same as Fig. 6 for Ni.

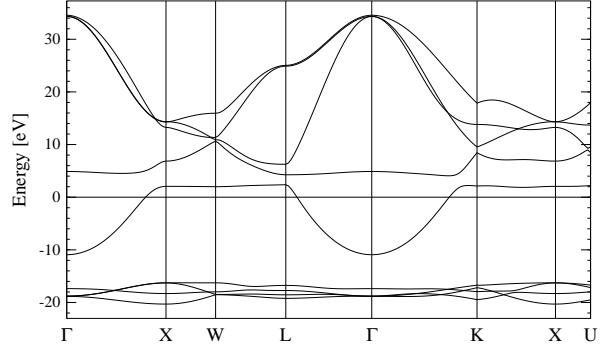


FIG. 13: Non-magnetic HFA-band structure for Co.

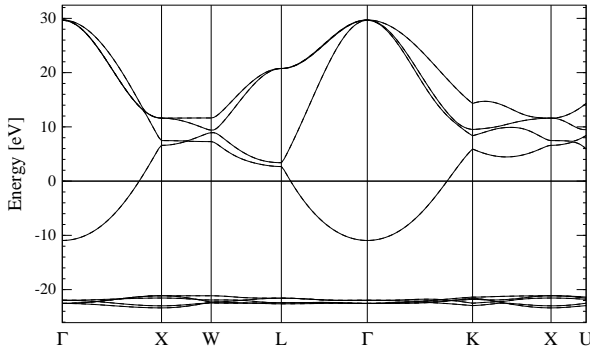


FIG. 11: The same as Fig. 5 for Cu.

netism. This can be seen already from the non-magnetic system Cu, for which the (fully occupied) 3d-bands also lie at about 22 eV below the Fermi level (see Figs. 11 and 12). To demonstrate this also for a system with a partially filled 3d-band we have done a non-magnetic Hartree-Fock-calculation for Co (by forcing equal occu-

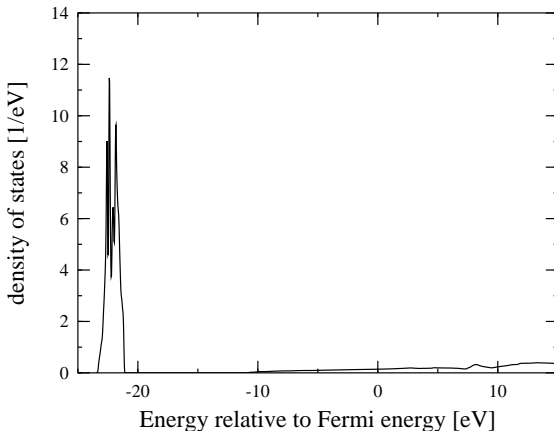


FIG. 12: The same as Fig. 6 for Cu.

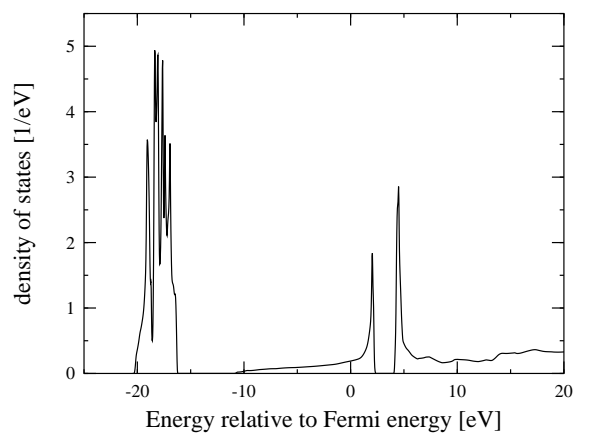


FIG. 14: Total density of states (of both degenerate spin directions) for Co obtained within the non-magnetic HFA-solution.

pation for both spin directions). The results for the band structure and the DOS are shown in Figs. 13,14. We observe again that the main part of the 3d-bands are well below the 4s-bands and Fermi level; note the hybridization gap caused by the unoccupied 3d-bands above the Fermi level.

VI. COMPARISON WITH ATOMIC HARTREE-FOCK RESULTS

We have seen in the previous section that one effect of the HFA calculation, when compared with the Hartree calculation, is the shift of the 3d-bands down (about 20 eV below the Fermi level and about 8–10 eV below the bottom of the 4sp-band). This shift of the d-bands is about the same energy as the Coulomb matrix elements U , and roughly agrees earlier atomic Hartree-Fock calculations^{14,15}, where the 3d-states are also about 10 eV below the 4s-states.

Because the inter-site hopping matrix elements in Table III are much smaller than the U -values one may consider an expansion in t/U , with the zeroth order ap-

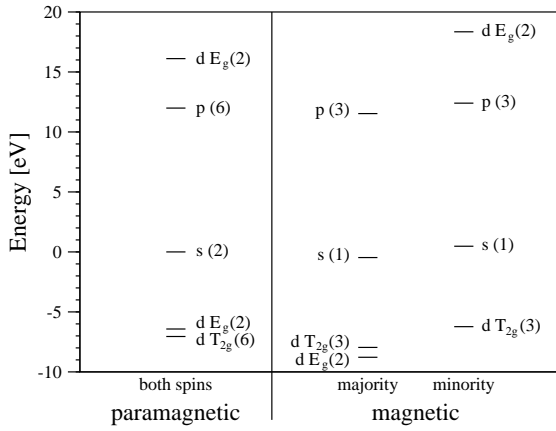


FIG. 15: Energy eigenvalues from quasi-atomic HFA calculation. The numbers in brackets indicate the degeneracy.

proximation to completely neglect hopping. Doing this, we have performed a quasi-atomic HFA calculation for Co, by including only the on-site one-particle and two-particle (Coulomb) matrix elements. The results are summarized in Fig. 15; the degeneracy of the different levels is also indicated. In the paramagnetic case, we find that the 3d-bands are below the 4s-bands (at the Fermi level) by about 6 to 7 eV, which is in rough agreement with the earlier atomic HFA results^{14,15}. The splitting between the occupied and unoccupied 3d-states is about 23 eV, which is the on-site U for Co. Magnetic HFA solutions are also found in the atomic limit for Co, as shown in the right panel of Fig. 15. The majority-spin 3d states (T_{2g} and E_g) are now completely filled and energetically lie lower than the corresponding non-magnetic HFA-states. But only the (3-fold degenerate) T_{2g} -states of the minority-spin electrons are filled whereas the E_g -states of the minority electrons are empty (and now even 26 eV above the occupied d-states). The additional energetical shifts between the occupied 3d-states in the paramagnetic and ferromagnetic atomic HFA solution are due to the exchange matrix elements J .

This behavior can qualitatively be understood within the framework of the following simple, analytically solvable model. Similar to the numerical HFA-results presented and discussed above, we neglect all intersite one-particle (hopping) and interaction matrix elements. Furthermore, we assume that we have diagonalized the one-particle Hamiltonian, taking into account only the atomic 3d-levels and assuming that the on-site one-particle diagonal matrix elements ε , the Coulomb matrix elements U , and the exchange matrix elements J are equal, i.e., that the 3d-levels are degenerate in the atomic limit with no crystal-field effects. Then the atomic part of the many-body Hamiltonian can be written as

$$H = \sum_{i\sigma} \varepsilon c_{i\sigma}^\dagger c_{i\sigma} + \frac{U}{2} \sum_{(i\sigma) \neq (j\sigma')} c_{i\sigma}^\dagger c_{i\sigma} c_{j\sigma'}^\dagger c_{j\sigma'}$$

$$+ \frac{J}{2} \sum_{i \neq j, \sigma\sigma'} c_{i\sigma}^\dagger c_{j\sigma'}^\dagger c_{i\sigma'} c_{j\sigma} \quad (19)$$

where $i, j \in \{0, \dots, 4\}$ denote the 5 (degenerate) 3d-states.

The standard Hartree-Fock decoupling leads to

$$H = \sum_{i\sigma} \left(\varepsilon + U \left[\sum_{j\sigma'} \langle c_{j\sigma'}^\dagger c_{j\sigma'} \rangle - \langle c_{i\sigma}^\dagger c_{i\sigma} \rangle \right] - J \sum_{j \neq i} \langle c_{j\sigma}^\dagger c_{j\sigma} \rangle \right) c_{i\sigma}^\dagger c_{i\sigma} . \quad (20)$$

Here we have assumed that the Hartree-Fock Hamiltonian has the same symmetry as the uncorrelated Hamiltonian, and hence off-diagonal expectation values $\langle c_{j\sigma'}^\dagger c_{i\sigma} \rangle$ for $(i\sigma) \neq (j\sigma')$ vanish. From this equation it is clear that the HF Hamiltonian can be written in terms of an effective one-particle energy

$$H = \sum_{i\sigma} \varepsilon_{i\sigma}^{\text{HFA}} c_{i\sigma}^\dagger c_{i\sigma} \quad (21)$$

where

$$\varepsilon_{i\sigma}^{\text{HFA}} = \varepsilon + U \left[\sum_{j\sigma'} \langle c_{j\sigma'}^\dagger c_{j\sigma'} \rangle - \langle c_{i\sigma}^\dagger c_{i\sigma} \rangle \right] - J \sum_{j \neq i} \langle c_{j\sigma}^\dagger c_{j\sigma} \rangle . \quad (22)$$

In the simple Hartree approximation (HA) the exchange decouplings are neglected, which means that all the decoupling terms with the negative sign would not occur. Therefore, the corresponding Hartree one-particle energies are given by

$$\varepsilon_{i\sigma}^{\text{HA}} = \varepsilon + U \sum_{j\sigma'} \langle c_{j\sigma'}^\dagger c_{j\sigma'} \rangle . \quad (23)$$

Comparing this result with the Hartree-Fock one-particle energies, we find that the HF occupied levels are shifted downwards by an amount of

$$U \langle c_{i\sigma}^\dagger c_{i\sigma} \rangle + J \sum_{j \neq i} \langle c_{j\sigma}^\dagger c_{j\sigma} \rangle \quad (24)$$

relative to the Hartree levels. Momentarily setting $J = 0$, we see that for N occupied levels the Hartree approximation gives the one-particle energies

$$\varepsilon_{i\sigma}^{\text{HA}} = \varepsilon + NU \quad (25)$$

whereas the HFA yields

$$\varepsilon_{i\sigma}^{\text{HFA}} = \varepsilon + (N - 1)U . \quad (26)$$

The occupied Hartree-Fock one-particle energies are lower than the corresponding Hartree one-particle energies by U , which is a consequence of the artificial and unphysical self-interaction still present in the Hartree approximation that is exactly cancelled in Hartree-Fock. This also explains why the Hartree-Fock bands are

shifted downwards from the Hartree bands by an energy of the amount U . One also sees from this simple atomic-limit Hartree-Fock model that the energy difference between the highest occupied and the lowest unoccupied effective Hartree-Fock one-particle energies is again essentially U , which is once more in agreement with our numerical results for the crystal and for the atom (cf. Fig.15). Note that we have ignored U_{sd} interactions, which cause an additional shift of d-bands below the s-bands by about an additional 10 eV in the full HFA calculations.

Taking into account the exchange interaction J again and denoting by N_σ the number of occupied states with spin σ (i.e. $N = N_\uparrow + N_\downarrow$) one obtains in HFA

$$\varepsilon_\sigma^{\text{HFA}} = \varepsilon + (N - 1)U - (N_\sigma - 1)J . \quad (27)$$

Then the total energy in HFA is given by

$$E_{\text{tot}} = N\varepsilon + \frac{N(N-1)}{2}U - \sum_\sigma \frac{N_\sigma(N_\sigma-1)}{2}J . \quad (28)$$

For the total energy we have added the necessary correction term to the sum of the occupied energy levels (much like the double counting term that shows up in band-structure calculations). Now for partially filled 3d-shells the occupation of the different spin directions may be different. Denoting $M = N_\uparrow - N_\downarrow$ we obtain for the total energy

$$E_{\text{tot}} = N\varepsilon + \frac{N(N-1)}{2}U - \frac{N^2 + M^2}{4}J + \frac{N}{2}J . \quad (29)$$

The magnetic ($M \neq 0$) total energy is lower than the nonmagnetic (consistent with Hund's rules).

Take once more Co with 8 3d-electrons. The paramagnetic (nonmagnetic) state has the occupations $N_\downarrow = N_\uparrow = 4$ ($N=8$ and $M=0$). For this configuration (corresponding to the left panel in Fig. 15) one obtains

$$E_{\text{tot}}^{(P)} = 8\varepsilon + 28U - 12J . \quad (30)$$

The Hund's rule magnetic solution has 3d-states of one spin-direction completely filled, i.e., $N_\uparrow = 5$ and $N_\downarrow = 3$ ($N=8$ and $M=2$). This gives

$$E_{\text{tot}}^{(M)} = 8\varepsilon + 28U - 13J . \quad (31)$$

Therefore, the magnetic configuration (with a magnetic moment of 2 for the atom) is energetically more favorable by J . Note also the exchange splitting in the occupied energy eigenvalues

$$\varepsilon_\downarrow - \varepsilon_\uparrow = 2J \quad (32)$$

and that our model would predict the unoccupied minority spin E_{2g} state to be $U + J$ higher in energy than the corresponding occupied majority spin state.

The simple model in this section differs from the results shown in Fig. 15 in that we have replaced the full matrix of U and J by scalar values for d-states only (ignoring s-d interactions, for example). However, it captures all of the important physics without attempting to be completely quantitative.

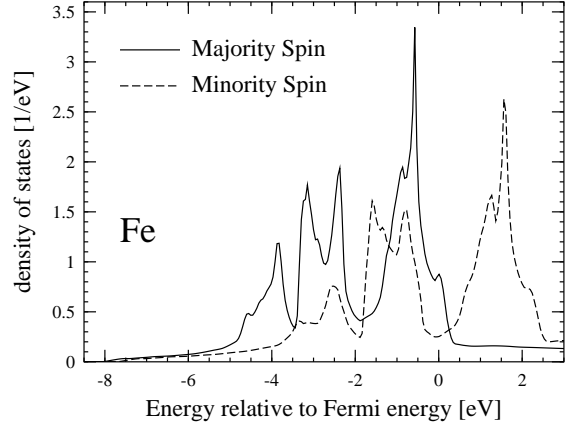


FIG. 16: Density of states (per spin direction) for Fe within the (unscreened) local spin-density approximation(LSDA); the full line shows the majority (spin up), the dashed line the minority spin contribution.

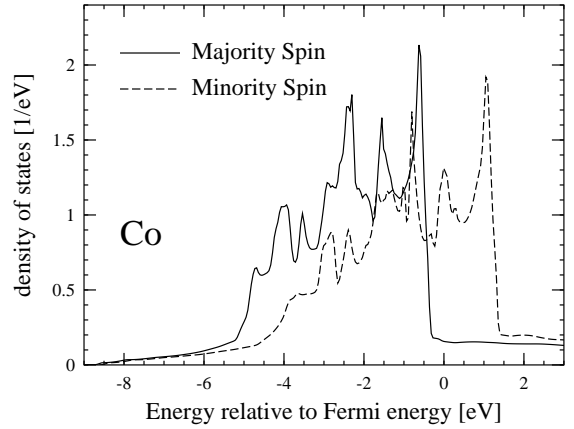


FIG. 17: The same as Fig. 16 for Co.

VII. COMPARISON WITH LSDA RESULTS

For comparison with the HFA results described in Section V we have also performed a standard local spin-density approximation (LSDA), ab-initio, band-structure calculation with the LMTO-ASA method. The results for the DOS are shown in Figs. 16–19. For the magnetic systems Fe, Co, and Ni one obtains also an exchange splitting and the prediction of magnetic solutions with magnetic moments of 2.18 for iron, 1.58 for Co, and 0.58 for Ni, which are in better agreement with experiment than the HFA results. This is consistent with the expectation that L(S)DA is tuned to accurately predict ground-state properties.

The energy spectra of the bands (DOS) are quite different from the HFA. For example, the 3d-bands now fall into the same energy region as the 4sp-bands, i.e., the LSDA-results are not so different from the Hartree-results. This means that the exchange-correlation energy leads only to a small shift of the 3d-bands downwards by

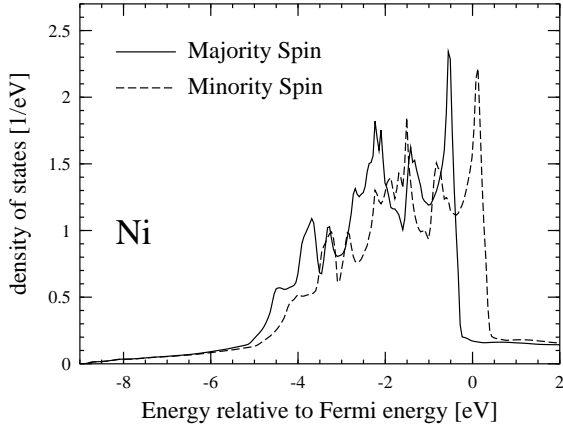


FIG. 18: The same as Fig. 16 for Ni.

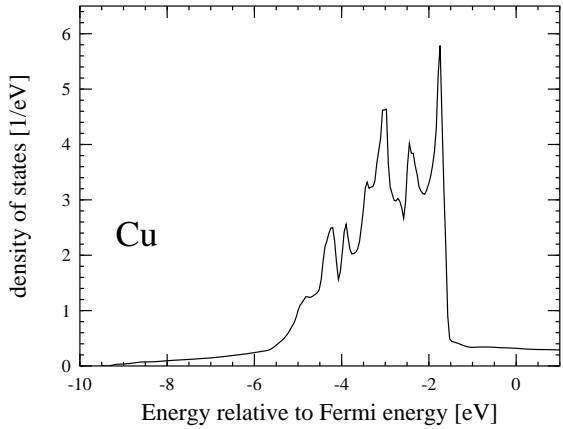


FIG. 19: Total density of states (of both degenerate spin directions) for Cu within the local density approximation(LSDA)

at most a few eV and a smaller exchange splitting (also of the magnitude of 1 eV) in the case of magnetic solutions. On the other hand, in the LSDA calculations the self-interaction terms are not completely canceled, i.e., an (unrealistic) self-interaction is included, which may lead to 3d bands that lie energetically too high, as discussed for the atomic limit in the previous section.

To see the effect of correlations within LSDA, we have also performed an exchange-only calculation for Co. The result is shown in Fig. 20. Obviously the (majority) d-bands lie lower than the ones in the full LSDA-calculation shown in Fig. 17. But the shift is of the magnitude of 1 eV only, i.e., very minimal when compared with the large drop in the full HFA. On the other hand, this exchange-only LSDA-result also does not contain self-interaction corrections, which are responsible for the large shift downwards of the d-bands. Nevertheless, the LSDA result indicates that a possible effect of correlations is to shift the 3d-bands up relative to exchange-only calculations, and hence one would expect a similar effect if correlations could be added to the full HFA-calculations.

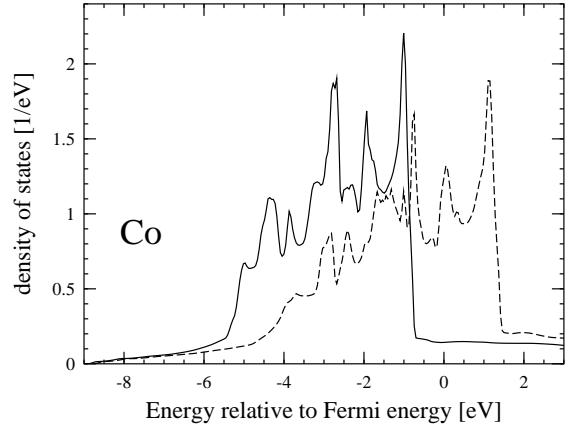


FIG. 20: Total density of states for Co within the "exchange-only" local density approximation(LSDA).

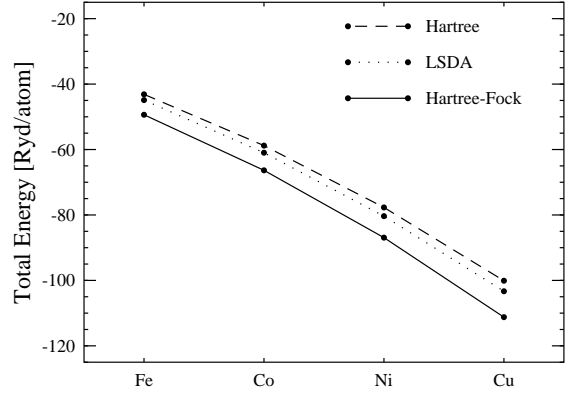


FIG. 21: Total ground state energy (of the valence electrons) obtained in Hartree-approximation, L(S)DA and HFA for the 3d transition metals Fe through Cu.

One can also calculate the total energy in the Hartree, HFA, and LSDA approximations. The results obtained for the four materials of interest are shown in Fig. 21. We see that the total energy is always significantly lower in HFA than in the Hartree approximation, which is expected because the HFA minimizes the total energy. The HFA total energy is also lower than the L(S)DA, and the LSDA result is lower than the simple Hartree result. Because of the unknown approximations that go into constructing L(S)DA, it is hard to guess ahead of time that this would be the case. However, it is well known that the L(S)DA approximation produces a bad total exchange-correlation energy; the reason why such good agreement with experiment is found is that relative exchange-correlation energies are nonetheless reasonably accurately calculated.

VIII. DISCUSSION AND CONCLUSION

In this paper we have presented the results of (unscreened) HFA calculations for the 3d transition metals Fe, Co, Ni and Cu. We obtain magnetic solutions for Fe, Co, and Ni with (slightly) too large magnetic moments when compared to experimental or LSDA results. The occupied HFA 3d-bands lie about 20 eV below the Fermi level (and the Hartree result), which is also the magnitude of the splitting between occupied and unoccupied 3d-bands and of the magnitude of the on-site Coulomb matrix element (the "Hubbard" U). This downwards shift of the HFA 3d-bands compared to the Hartree- and L(S)DA-3d-bands can be understood as due to the self-interaction correction of HFA.

One may argue that these results are not surprising and an artifact of using the unscreened HFA. Our ab-initio calculation of the direct Coulomb matrix elements yields large values of the magnitude of 20 eV. Therefore the Coulomb energies are large for these materials and HFA can be considered to be an approximation for the selfenergy which is correct only in linear order in the Coulomb interaction. But for these large values of the U -terms HFA is certainly not sufficient but one has to apply better many-body approximations. One should apply systematic extensions of HFA, which within the standard perturbational approach can be represented by (a resummation of an infinite series of) Feynman diagrams, or one can try to apply the recently so successful non-perturbational many-body schemes like "dynamical mean field theory" (DMFT)¹⁶ or variational (Gutzwiller) approaches¹⁷. The simplest standard diagram series are the bubble diagrams leading essentially to the "random phase approximation" (RPA). This means just a renormalization of the interaction line, i.e. the pure "naked" Coulomb interaction has to be replaced by a "dressed" interaction. Or in other words, the exchange (Fock) con-

tribution has not to be calculated with the bare Coulomb matrix elements but with screened Coulomb matrix elements. Probably the non-perturbational schemes like DMFT are also only applicable for screened Coulomb matrix elements.

To summarize, the new many-body ab-initio approach proposed in Ref. 1 is applicable to real materials. Maximally localized Wannier functions and their one- and two-particle matrix elements can be calculated from first principles so as to obtain a many-body multi-band Hamiltonian in second quantization. Standard methods of many-body theory can then be applied to this Hamiltonian. The simplest approximation (HFA) is unreliable, because the large Coulomb matrix elements are unscreened. Therefore, in the future better many-body approximations should be used. Within the standard Feynman diagram approach the most straightforward next step consists in a summation of bubble diagrams leading to a renormalized (screened) Coulomb interaction. This requires calculating the exchange contribution not with the bare but with a screened Coulomb interaction. To take into account the effects of screening one has to calculate the charge susceptibility and the (static) dielectric constant, which can be done within a generalized Lindhard theory, for instance.

Acknowledgments

This work has been supported by a grant from the Deutsche Forschungsgemeinschaft No. Cz/31-12-1. It was also partially supported by the Department of Energy under contract W-7405-ENG-36. This research used resources of the National Energy Research Scientific Computing Center, which is supported by the Office of Science of the U.S. Department of Energy under Contract No. DE-AC03-76SF00098.

¹ I. Schnell, G. Czycholl, R.C. Albers, Phys. Rev. B, preceeding paper (2003)

² N. Marzari and D. Vanderbilt, Phys. Rev. B **56**, 12847 (1997).

³ H.L. Skriver, *The LMTO Method* (Springer-Verlag, Heidelberg 1984)

⁴ R.M. Dreizler, E.K.U. Gross, *Density Functional Theory*, Springer (Berlin, Heidelberg, New York 1990)

⁵ H. Eschrig, *The Fundamentals of Density Functional Theory* (Teubner Stuttgart, Leipzig 1996)

⁶ G. Stollhoff, Phys. Rev. B **58**, 9826 (1998)

⁷ G.D. Mahan, *Many-Particle Physics* (Plenum Press New York 1990)

⁸ C. Pisani, R. Dovesi, C. Roetti, *Hartree-Fock Ab Initio Treatment of Crystalline Systems* (Lecture Notes in Chemistry, Vol. 48, Springer-Verlag Berlin Heidelberg 1988); C. Pisani, *Quantum-Mechanical Ab-initio calculation of the Properties of Crystalline Materials*, Lecture Notes in Chemistry, Vol. 67, Springer Verlag, Heidelberg, 1996

⁹ H.J. Monkhorst, Phys. Rev. B **20**, 1504 (1979)

¹⁰ R. Dovesi, C. Pisani, F. Ricca, C. Roetti, Phys. Rev. B **25**, 3731 (1982)

¹¹ O.K. Andersen, Phys. Rev. B **12**, 3060 (1975)

¹² I. Schnell, G. Czycholl, R.C. Albers, Phys. Rev. B **65**, 075103 (2002)

¹³ J.C. Slater, Phys. Rev. **34**, 1293 (1929)

¹⁴ R.E. Watson, Phys. Rev. **118**, 1036 (1959); **119**, 1934 (1959)

¹⁵ L. Hodges, R.E. Watson, H. Ehrenreich, Phys. Rev. B **5**, 3953 (1972)

¹⁶ For a review see: A. Georges, G. Kotliar, W. Krauth, M.J. Rozenberg, Rev. Mod. Phys. **68**, 13 (1996)

¹⁷ W. Weber, J. Bünenmann, F. Gebhard, in *Band-Ferromagnetism* (Lecture Notes in Physics, Vol. 580, p.9 (eds.: K. Baberschke, M. Donath, W. Nolting, Springer Berlin 2001); J. Bünenmann, W. Weber, F. Gebhard, Phys. Rev. B **57**, 6896 (1998)